Adaptive Learning of Inland Ship Power Propulsion under Environmental Disturbances

Dann, Nicolas; Segovia, Pablo; Reppa, Vasso

DOI
10.1016/j.ifacol.2022.10.400

Publication date
2022

Document Version
Final published version

Published in
IFAC-PapersOnline

Available online at www.sciencedirect.com

ScienceDirect

IFAC PapersOnline CONFERENCE PAPER ARCHIVE

IFAC PapersOnLine 55-31 (2022) 1–6

Adaptive Learning of Inland Ship Power Propulsion under Environmental Disturbances ⋆

Nicolas Dann, Pablo Segovia, Vasso Reppa

Department of Maritime and Transport Technology, Delft University of Technology, Delft, The Netherlands (e-mail: {n.dannruiz@student., p.segoviacastillo@, v.reppa@}tudelft.nl).

Abstract: This paper presents an adaptive approximation-based scheme for learning a partially known ship power propulsion plant under various environmental conditions. Considering the effect of water depth on the engine power, a dynamic model is defined comprised of the engine dynamics and the 1-DoF ship manoeuvring dynamics. The modelling challenge is the determination of ship resistance. To meet this challenge analytical modelling of ship resistance is combined with an error-filtering online learning (EFOL) scheme for computing an approximation of the unmodeled part of ship resistance related to wind and air. After simulations under multiple weather conditions, the trained model was demonstrated to efficiently estimate the unmodelled part of the ship resistance for an inland vessel.

Keywords: On-line learning scheme, surface vehicles, speed-power prediction, ship resistance, shallow water.

1. INTRODUCTION

Increasing environmental concerns and global warming have prompted international regulations on energy efficiency for ocean-going vessels. According to the International Maritime Organisation (IMO), maritime transport emits around 940 million tonnes of CO_2 annually and is responsible for about 2.5% of global greenhouse gas emissions (GHGs). At the current pace, the annual GHGs from maritime transport in 2050 are estimated to exceed the total shipping emissions in 2008 by 90-130%, undermining the 50% reduction imposed by the Paris Agreement (IMO, 2020). Thereby, the shipping industry is striving to employ measures for fuel efficiency, that depends on the powering performance of vessels.

Propulsion performance is a measure of the energy consumption at a certain state, and can be studied as the relation between a ship's speed and the required propulsion power (Pedersen and Larsen, 2009). During the lifetime of a ship, speed is bound to decrease for the same input powers as a result of performance reduction. As ships are subject to external factors such as wind and waves, it is unlikely that two identical operational scenarios occur, making the estimation of propulsion performance complex.

Analytical mathematical models have been predominantly used to address powering performance by quantifying the speed-power relation based on speed loss due to ship resistance. For ocean-going vessels, a primarily utilised calculation is the procedure presented in Holtrop (1984) and recently validated in Nikolopoulos and Boulougouris (2019) and Grabowska and Szczuko (2015). In regards to inland waterways, shallow water depths significantly increase ship resistance, making propulsion estimation highly intricate (Zeng, 2019). A common practice in the literature is to apply a correction on either the propulsion power or the ship velocity of a deepwater method. The most renowned shallow water resistance correction methods can be argued to be the ones presented in Raven (2016), Schlichting (1934), and Lackenby (1963).

Limitations in terms of the accuracy and applicability of analytical methods mainly rely on their empirical nature. As a result of being based on model tests carried out under design conditions, when implemented in real-life a rough estimate of the actual propulsion performance is achieved (Pedersen and Larsen, 2009). Furthermore, as calculations are based on the parametrisation of the hull shape, solely ships within a set of specification limits may be considered. According to Bertram (2012), analytical methods are thus bound to become invalid for modern vessel shapes. With respect to inland waterways, Zeng (2019) and Schlichting (1934) have further claimed shallow water methods to be physically weak and questionable given their dependency on deepwater calculations.

With computational techniques becoming increasingly powerful and efficient, data-driven methods for analysing the powering performance of ships using measurement data have attracted increased attention (Yoo and Kim, 2019). Particularly, machine learning (ML) techniques have been shown to improve the accuracy of propulsion performance estimation. In the paper by de Geus-Moussault et al. (2021), an artificial neural network (ANN)

⋆ This research is supported by the project "Novel inland waterway transport concepts for moving freight effectively (NOVIMOVE)". Funded by the European Union's Horizon 2020 research and innovation programme under grant agreement No 858508 and the Researchlab Autonomous Shipping (RAS) of Delft University of Technology.

10.1016/j.ifacol.2022.10.400

and a convolutional neural network (CNN) were developed for the speed prediction of ocean-going ships, concluding on their superior prediction accuracy, particularly by the ANN. Similarly, Moreira et al. (2021) introduced an ANN for propulsion performance estimation by predicting speed and fuel consumption, while Abebe et al. (2020) implemented a variety of regression methods such as forest and gradient boosting regressors. The shorter computation time and higher accuracy of ML techniques compared to analytical methods make ML an appealing technology, particularly given its easy implementation on board any ship comprising the designated set of sensors (Abebe et al., 2020).

Although ML techniques can be powerful in estimating the power propulsion performance of a ship, deriving guarantees for their performance considering properties like convergence is not possible. There has been significant research activity on techniques that integrate model-based and data-driven techniques in adaptive learning schemes (Farrell and Polycarpou, 2006), (Reppa et al., 2016). These schemes are developed by carrying out stability analysis that offers valuable information about the properties of the adaptive scheme and a systematic way to select the design parameters.

The goal and the main contributions of this work are: (1) the analytical ship power propulsion modelling for inland waterways based on state-of-the-art propulsion and resistance calculation methods, and (2) a novel error-filtering online learning (EFOL) scheme based on a radial basis function neural network (RBFNN). The EFOL scheme integrates an adaptive nonlinear approximator of the unmodelled effect of ship resistance and an estimator that utilizes analytical models (i.e. prior knowledge) of the ship power propulsion and filters some signals to limit the effects of noise. On a wider note, this paper aims to contribute towards the development of a tool to be implemented onboard a ship for real-time propulsion performance prediction.

This paper is organized as follows. The analytical propulsion and resistance models are presented in Sections 2 and 3, respectively. In Section 4, the developed adaptive learning scheme is presented, which is later tested in a case study in Section 5. Finally, Section 6 addresses concluding remarks and future research avenues.

2. SHIP POWER PROPULSION MODEL

In this work, ship propulsion is considered to be described based on the following equations (Yoo and Kim, 2017):

$$\begin{aligned}
&\text{Engine Speed :} && n_b = G_R n_p, && \text{(1a)}\\
&\text{Engine power :} && P = 2\pi n_b Q_B, && \text{(1b)}\\
&\text{Propeller thrust :} && T = K_T \rho n_p^2 D^4, && \text{(1c)}\\
&\text{Propeller torque :} && Q_p = K_Q \rho n_p^2 D^5, && \text{(1d)}\\
&\text{Engine dynamics :} && 2\pi I_p \dot{n_p} = \eta_S G_R Q_B - Q_p, && \text{(1e)}\\
&\text{Ship dynamics :} && (m+m_a)\dot{V_S} = T - R, && \text{(1f)}\\
&\text{Ship resistance :} && R = f_r(V_S, W), && \text{(1g)}
\end{aligned}$$

where G_R is the gear ratio between the propeller shaft and ship engine [-], n_p is the propeller speed [Hz], n_b is the engine speed [Hz], Q_B is the engine torque [N $\cdot$ m], ρ is the density of water [kg/m^3], D is the propeller diameter [m], I_p is the total inertia of the propeller [kg $\cdot$ m^2], η_S is the mechanical efficiency from the engine to the propeller [-], Q_p is the propeller torque [N $\cdot$ m], m is the ship's mass [kg], m_a is the ship's added mass [kg], V_S is the ship speed through water [m/s], and R is the ship resistance [N]. The latter will be further derived as a function f_r of the ship speed V_S and wind conditions W in Section 3. In this paper, the inland vessel and propeller parameters of *"Ship 2"* presented in the study by Nuij (2021) will be considered. Based on equations (1a)-(1g), the following dynamic model is derived:

$$\begin{aligned}
\dot{n_p} &= \frac{\eta_S}{4\pi^2 I_p}\frac{P}{n_p} - \frac{K_Q \rho D^5}{2\pi I_p} {n_p}^2\\
\dot{V_S} &= \frac{1}{m+m_a} K_T \rho D^4 {n_p}^2 - \frac{1}{m+m_a} f_r(V_S, W).
\end{aligned} \tag{2}$$

Ship manoeuvring and its required set of sensors are considered out of the scope of this study, therefore simplifying ship motions to 1 DoF, such that lateral (i.e sway), vertical (i.e heave), and rotational motions are neglected.
In the case of shallow water, the water depth affects the ship's propulsion performance. This is considered by correcting the engine power P [W] in (2) to incorporate the power increase effects of shallow water operation as (Raven, 2016):

$$P \rightarrow \frac{P}{R_{sink}} - \frac{\Delta R_V V_S}{\eta_{Did}}. \tag{3}$$

Thereafter, (2) becomes:

$$\dot{n_p} = \frac{\eta_S}{4\pi^2 I_p R_{sink}(H)}\frac{P}{n_p} - \frac{\eta_S \Delta R_V(H)}{4\pi^2 I_p \eta_{Did}}\frac{V_S}{n_p} - \frac{K_Q \rho D^5}{2\pi I_p} {n_p}^2$$

$$\dot{V_S} = \frac{1}{m+m_a} K_T \rho D^4 {n_p}^2 - \frac{1}{m+m_a} f_r(V_S, W), \tag{4}$$

where the viscous resistance increase due to shallow water, the resistance due to sinkage, and the propulsive efficiency coefficient in ideal condition are respectively defined as:

$$\Delta R_V = R_{V deep} 0.57 (T/H)^{1.79}, \tag{5}$$

$$R_{sink} = (1 + \delta\nabla)^{2/3}, \tag{6}$$

$$\eta_{Did} = \eta_O \eta_{Rid} \frac{1-\tau_{id}}{1-w_{Sid}}, \tag{7}$$

where T is the ship draft [m], H is the water depth [m], τ_{id} is the ideal thrust deduction factor [-], w_{id} is the ideal full-scale wake fraction [-], η_O is the propeller's open-water efficiency [-], and η_{Rid} is the ideal factor for relative rotative efficiency [-]. The deepwater viscous resistance and additional displacement due to sinkage are calculated as:

$$R_{V deep} = C'_v \frac{1}{2} \rho V_S^2 S, \tag{8}$$

$$\delta\nabla = d(sinkage) A_W / \nabla, \tag{9}$$

where C'_v is the viscous resistance coefficient [-] derived as a function of the Reynold's number (Raven, 2016), A_W is the frontal projected area [m^2], and $d(sinkage)$ [m] is determined as:

$$d(sinkage) = 1.46 \frac{B T_M C_B}{L_{pp}} \left[\frac{Fr_h^2}{\sqrt{1-Fr_h^2}} - \frac{Fr_{hd}^2}{\sqrt{1-Fr_{hd}^2}} \right], \tag{10}$$

with:

$$Fr_{hd} = \frac{V_S}{\sqrt{0.3gL_{pp}}} \qquad Fr_h = \frac{V_S}{\sqrt{gH}}, \tag{11}$$

where L_{pp} denotes the ship's length between perpendiculars [m], B is the ship molded beam [m], T_M is the draught at midship [m], C_B is the Block coefficient [-], and g is the gravitational acceleration constant [m/s^2].
The objective of this work is to define the ship resistance in (1g) by integrating analytical modelling and an adaptive learning scheme.

3. ANALYTICAL MODELLING OF SHIP RESISTANCE

The deepwater resistance method derived in Holtrop (1984) computes a dimensional total resistance [N] (12) based on the ship's speed and its principal dimensions.

$$R = (1+k)R_F + R_{APP} + R_W + R_B + R_{TR} + R_A + R_{AA}. \tag{12}$$

The frictional resistance R_F (13) is multiplied by the hull form factor k and can be computed as:

$$R_F = \frac{1}{2}\rho V_S^2 S C_F, \tag{13}$$

where S is the wetted surface area [m^2] and C_F is the model–ship correlation line coefficient [-], which may be calculated as a function of the Reynold's number Re (1957 ITTC Standards):

$$C_F = \frac{0.075}{(log_{10}Re - 2)^2}. \tag{14}$$

The appendage resistance R_{APP} is calculated as the sum of the resistance due to the appendages and the bow thruster resistance, quantified by the expression:

$$R_{APP} = \frac{1}{2}\rho V_S^2 \frac{\sum_i (1+k_2) S_{APP_i}}{\sum_i S_{APP_i}} C_F \sum_i S_{APP_i} + R_{TH}, \tag{15}$$

where the $(1 + k_2)$ values for each appendage i are presented in Holtrop (1984), S_{APP_i} denotes the surface area of each considered appendage i [m^2], and the resistance due to the bow thruster tunnel opening R_{TH} is computed as:

$$R_{TH} = \rho V_S^2 \pi d_{TH}^2 C_{D,TH}, \tag{16}$$

with the drag coefficient $C_{D,TH}$ for the thruster tunnel assuming values between 0.003 and 0.012 (Birk, 2019), and with d_{TH} being the thruster tunnel's diameter [m].
Furthermore, the wave-making resistance R_W is estimated as a function of the Froude number F_r [-] (Holtrop, 1984):

- for $Fr < 0.4$:
$$R_{Wa}(Fr) = c_1 c_2 c_5 \rho g V e^{\left[m_1 Fr^d + m_4 cos\left(\lambda Fr^{-2}\right)\right]}, \tag{17}$$
- for $Fr > 0.55$:
$$R_{Wb}(Fr) = c_{17} c_2 c_5 \rho g V e^{\left[m_3 Fr^d + m_4 cos\left(\lambda Fr^{-2}\right)\right]}, \tag{18}$$
- for $0.4 < Fr \leq 0.55$, an interpolation of (17) and (18) applies:

$$R_W(Fr) = R_{Wa}(0.4) + \frac{(20Fr - 8)}{3}\left[R_{Wb}(0.55) - R_{Wa}(0.4)\right], \tag{19}$$

where the parameters denoted c and m are dimensionless calculation coefficients presented in Holtrop (1984).

The additional bulbous bow resistance R_B is computed according to:

$$R_B = 0.11\rho g(\sqrt{A_{BT}})^3 \frac{{Fr_i}^3}{1 + {Fr_i}^2} e^{(-3.0 {P_B}^{-2})}, \tag{20}$$

where Fr_i denotes the immersion Froude number [-].
The immersed transom resistance R_{TR} is further computed as:

$$R_{TR} = \frac{1}{2}\rho {V_S}^2 A_T c_6. \tag{21}$$

Additionally, the Holtrop (1984) method accounts for a correlation allowance resistance R_A to include the effects of roughness and additional phenomena not captured in the previous resistance components:

$$R_A = \frac{1}{2}\rho {V_S}^2 (C_A + \Delta C_A)\left[S + \sum_i S_{APP_i}\right], \tag{22}$$

where C_A and ΔC_A are correlation allowance coefficients [-] specified in Holtrop (1984).
Finally, the shape of the ship has a direct influence on its aerodynamics, which is quantified as air and wind resistance R_{AA}, defined by:

$$R_{AA} = \frac{1}{2}\rho_A V_{w,ref}^2 C_w A_W, \tag{23}$$

where C_w is the wind coefficient [-] and $V_{w,ref}$ is the relative wind speed [m/s], calculated as the difference between the ship's forward speed through water V_S and the wind velocity u_w in the x-direction [m/s]:

$$u_w = V_w cos(\psi_w), \tag{24}$$

where V_w is the sensed wind speed [m/s] and ψ_w denotes the wind direction, with $\psi_w = 0$ indicating headwind.
The complexity of parameterising a ship's geometry and computing the frontal projected area A_W using analytical methods makes R_{AA} highly intricate to estimate. Thereafter, R_{AA} will be considered as the function to be approximated, with the objective of learning the unknown relation between its inputs through an approximation scheme.

4. ADAPTIVE LEARNING SCHEME

The dynamic system in (4) can be re-written in state-space form by considering $x = [n_p V_S]^T$ and $u(t) = P$ as:

$$\begin{aligned}
\dot{x_1} &= \frac{\eta_S}{4\pi^2 I_p}\left(\frac{1}{R_{sink}(H)}\frac{u}{x_1} - \frac{\Delta R_V(H)}{\eta_{Did}}\frac{x_2}{x_1}\right) - \frac{K_Q \rho D^5}{2\pi I_p} x_1^2 \\
\dot{x_2} &= \frac{1}{m + m_a} K_T \rho D^4 {x_1}^2 - \frac{1}{m + m_a}[(1+k)R_F + R_{APP} \\
&\quad + R_W + R_B + R_{TR} + R_A] - \frac{1}{m + m_a} R_{AA}.
\end{aligned} \tag{25}$$

Equation (25) can be expressed as:

$$\dot{x_1} = f_{0,1}(x_1, x_2, u, d_3), \tag{26a}$$
$$\dot{x_2} = f_{0,2}(x_1, x_2) + f_2^*(x_2, d_1, d_2), \tag{26b}$$

where $f_{0,1}$ and $f_{0,2}$ are considered as known functions, while f_2^* is an unknown function to be learned. The disturbance due to V_w, ψ_w, and H are denoted d_1, d_2, and d_3, respectively.
An adaptive learning scheme is designed considering only (26b) since (26a) does not contain any uncertainty. In

addition, it is assumed that x_1, x_2, d_1, d_2, d_3 are all measured and the output of the sensors are:

$$\begin{aligned} y_1 &= x_1 + w_1 \\ y_2 &= x_2 + w_2 \end{aligned}, \qquad \begin{aligned} y_{d1} &= d_1 + w_3 \\ y_{d2} &= d_2 + w_4, \\ y_{d3} &= d_3 + w_5 \end{aligned} \tag{27}$$

where w denotes sensor measurement uncertainty. The states x_1 and x_2 can be measured by a differential GPS and an RPM sensor, respectively. In regards to the disturbances, d_1 and d_2 can be respectively measured by an anemometer and weathervane, while an echo sounder can be used to measure d_3.
The developed learning scheme is comprised of a parametric model and an error filtering online learning scheme.

4.1 Parametric Model

The parametric model is defined as:

$$\chi_2(t) = \hat{f}_2\left(x_2(t); \theta^*\right) + \delta_2(t), \tag{28}$$

where $\chi_2(t)$ is given by:

$$\chi_2(t) = \dot{x}_2(t) - f_{0,2}(x_1(t), x_2(t)), \tag{29}$$

and $\hat{f}_2$ is an adaptive approximation model (e.g radial basis function, sigmoidal neural network) which, based on unknown parameter weights θ_i^*, intends to decrease the minimum functional approximation error (MFAE) $\delta_2(t)$, defined as:

$$\delta_2(t) = f_2^*(x_2(t), d_1(t), d_2(t)) - \hat{f}_2(x_2(t); \theta^*). \tag{30}$$

4.2 Error Filtering Online Learning Scheme

Due to the fact that $\dot{x}_2$ is not available for measurement, a filtering technique is applied. By filtering both sides of (28) with a first-order filter, it yields:

$$\begin{aligned} \hat{\chi}_2(t) &= \frac{\lambda s}{s+\lambda}\left[x_2\right] - \frac{\lambda}{s+\lambda}\left[f_{0,2}(x_1, x_2)\right] \\ \hat{\chi}_2(t) &= \frac{\lambda}{s+\lambda}\left[\hat{f}_2(x_2(t); \theta^*)\right] + \hat{\delta}_2(t), \end{aligned} \tag{31}$$

where $\hat{\delta}_2(t)$ is the filtered version of the MFAE and s is the Laplace operator. The filters are described as transfer functions, using the relation $\dot{x_2} = s[x_2(t)]$. In this work, a linearly parametrized approximator is considered, i.e,

$$\hat{f}_2(x_2(t); \theta^*) = \sum_{i=1}^{q_\theta} \theta_i^* \phi_i(x_2(t)). \tag{32}$$

The unknown parameters θ_i^* are the adjustable parameters that minimise the MFAE and ϕ_i denotes an element of the regression vector. Considering the measurements of x_2, the EFOL scheme is designed as:

$$\begin{aligned} \hat{\chi}_2 &= \frac{\lambda s}{s+\lambda}\left[y_2\right] - \frac{\lambda}{s+\lambda}\left[f_{0,2}(y_1, y_2)\right] \\ \hat{\chi}_2 &= \frac{\lambda}{s+\lambda}\left[\theta^T \phi(y_2)\right], \end{aligned} \tag{33}$$

The structure of the implemented EFOL scheme is presented in Fig. 1.

4.3 Adaptive Law

The update law for the unknown set of parameters $\theta^*(t)$ must be further established. For this purpose, a linearly parametrized RBFNN approximator is implemented.

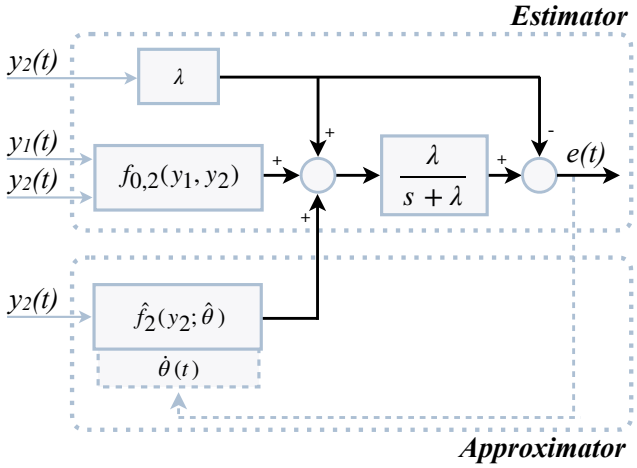

Fig. 1: Block diagram configuration of the EFOL scheme

Applications of RBFs in on-line learning approximation schemes can be seen in the works of Liu et al. (2021), Zhang (2016), Wu et al. (2012), and Gorinevsky (1993). In this paper, Gaussian RBFs will be introduced, redefining (32) as:

$$\hat{f}_2(x_2(t); \theta^*) = \theta^{*T} \phi(x, c, \sigma), \tag{34}$$

where the regression vector $\phi(x, c, \sigma)$ consists of Gaussian radial basis functions, with each RBF i being defined as:

$$\phi_i(x, c, \sigma) = exp(-\frac{1}{2}\frac{||x - c_i||^2}{\sigma^2}), \tag{35}$$

where c_i denotes the centre location for the $i-th$ Gaussian function and σ is the standard deviation or spread of the functions. To balance the trade-off between computational complexity and prediction accuracy, 12 neurons are considered, that is, $i \in \{1, ..., 12\}$. To increase the approximation accuracy, the fixed centre locations for the RBFs are evenly spaced over the operating velocity range of x_2, which is found to be $\{0, 5.5\}$, while the spread is tuned to $\sigma = 0.61$ for all RBFs using a brute-force approach.
In regards to learning, the output error signal of the scheme $e(t) = \hat{\chi}_2(t) - \chi_2(t)$ is used to adjust the parameter weights of the RBFNN. The Lyapunov synthesis method is typically utilised for EFOL schemes given its inherent stability properties (Farrell and Polycarpou, 2006). The following parameter adaptive law is thus derived for θ:

$$\dot{\hat{\theta}} = -\Gamma e(t) \phi(y_2, c, \sigma), \tag{36}$$

where Γ denotes the adaptive gain matrix, or learning rate, which will be simplified to $\Gamma = \gamma I$, implying that each element in $\theta(t)$ uses the same adaptive gain.

5. SIMULATION EXPERIMENT

5.1 Case Study

The inland vessel and propeller parameters of *"Ship 2"* studied in Nuij (2021) are used for this case study. The value of the design parameter λ is set to 1, while the efficiency coefficients are set to: $\eta_S = 0.95$, $\eta_{Did} = 0.95$, $\eta_O = 0.37$. The thrust, torque, wind resistance, and bow thruster coefficients are set to: $k_T = 0.1965$, $k_Q = 0.03316$, $C_w = 0.6$, and $C_{D,TH} = 0.07$. Furthermore, the mass of the ship is assumed to be $m = 10^6 kg$ while the added mass m_a is neglected.

In regards to training the RBFNN, the root mean square error (RMSE) of the prediction $\hat{f}_2$ with respect to f_2^* is used to define the scheme's accuracy:

$$RMSE = \sqrt{\frac{\sum_{i=1}^{N}(x_{2,i} - \hat{x}_{2,i})^2}{N}}, \quad (37)$$

where N is the number of data points, $x_{2,i}$ are the actual values of f_2^*, and $\hat{x}_{2,i}$ are the estimated values by $\hat{f}_2$. To optimise the training process, the EFOL scheme was run for a range of values of $\gamma = \{0.05, 0.1, ..., 1\}$ for 40 epochs each, and input power and disturbances $P = 600kW$ and $d = [0, 0, 4.5]$. On the one hand, small learning rates can cause the process of learning to get stuck, whereas, on the other hand, large learning rates can cause the model to converge quickly to a sub-optimal solution. A value of $\gamma = 0.3$ was found to increase this trade-off, and was used to train the model for 400 epochs.

5.2 Design of the Experiment

An experimental scenario aiming to mimic realistic wind conditions was designed to test the trained model. Medium-scale winds of up to 36km/h in the form of wind gusts were replicated by introducing a pulse and a ramp function for the sensed wind speed signal $y_{d1}(t)$ (Fig. 2). To imitate sensor noise, Gaussian white noise was introduced. White noise is expressed by a sequence of Gaussian variables, with their variance reflecting the power or intensity at each time step (Miller and Childers, 2012). A power of $E = 10^{-4}$ was selected, corresponding to a standard deviation of $0.01N$. Gaussian white noise was introduced to the sensed input signals $y_{d1}(t)$, $y_{d2}(t)$, and $y_{d3}(t)$. Furthermore, headwind ($d_2 = 0$) together with an input power of $u = 600kW$ were considered. The simulation of the EFOL scheme was then run for $10^4 s$.

5.3 Results and Discussion

The resulting approximation of the unknown function $f_2^*(t)$ by the function approximator $\hat{f}_2(t)$ and the error signal of the EFOL scheme $e(t)$ are plotted in Fig. 3(a) and Fig. 3(b) for the pulse and ramp $y_{d1}(t)$ inputs, respectively. In the plots, $f_2^*(t)$ can be seen to be closely replicated by the approximator function $\hat{f}_2(t)$, with the latter showing slight fluctuations due to sensor measurement noise.

For a pulse wind input signal (Fig. 3(a)), a total RMSE of $11.5329N$ is obtained, caused by overshoots of $\hat{f}_2(t)$ at the pulse input changes of $y_{d1}(t)$ and by approximation error due to sensor noise. Nevertheless, the error signal rapidly decreases after each overshoot, with each spike elapsing around 3 seconds.

In the case of $y_{d1}(t)$ being described by a ramp function (Fig. 3(b)), a smaller RMSE of $10.0073N$ is obtained, reflected in a smooth approximation of the unknown function $f_2^*(t)$. Note that, despite an increase in the sensed wind speed $d_1(t)$, the unknown air resistance $f_2^*(t)$ decreases at around halfway of the function's ramps. This is a result of R_{AA} being computed based on the wind speed relative to the ship's velocity. In reality, sensed wind should increase with forward ship motion, which was not accounted for in the theoretical $y_{d1}(t)$ signal.

In essence, the obtained results show the ability of the learning model to rapidly adapt to a varying input and closely learn the unknown system dynamics. Given the magnitude of the resistance values at hand, the obtained RMSE values can be argued to be significantly small.

6. CONCLUSIONS AND FURTHER RESEARCH

This paper studied the speed-power prediction of inland ships, a fundamental aspect of their powering performance, for which an approach combining an EFOL and a RBFNN was proposed. Considering a partially-known system, a set of dynamic equations were derived analytically for the known fraction of the system, while the air and wind resistance was considered an unknown function of onboard sensor measurements.

Simulation experiments indicate that the proposed method can closely approximate unknown dynamics, presenting itself as a feasible speed-power approximation model. For future validation, the model could be tested using real sensor data. This work allows for a variety of further extensions, such as considering the influence of ship manoeuvring by including the set of sensors required to describe ship motion in 6 DoFs.

REFERENCES

Abebe, M., Shin, Y., Noh, Y., Lee, S., and Lee, I. (2020). Machine learning approaches for ship speed prediction towards energy efficient shipping. *Applied Sciences*, 10(7), 2325.

Bertram, V. (2012). *Practical ship hydrodynamics*. Elsevier.

Birk, L. (2019). *Fundamentals of Ship Hydrodynamics: Fluid Mechanics, Ship Resistance and Propulsion*. John Wiley & Sons.

de Geus-Moussault, S., Buis, M., and Koelman, H. (2021). A convolutional neural network developed to predict speed using operational data. In *COMPIT'21: 20th International Conference on Computer and IT Applications in the Maritime Industries*, 246–264. Technische Universität Hamburg-Harburg.

Farrell, J.A. and Polycarpou, M.M. (2006). *Adaptive approximation based control: unifying neural, fuzzy and traditional adaptive approximation approaches*, volume 48. John Wiley & Sons.

Gorinevsky, D.M. (1993). Adaptive learning control using affine radial basis function network approximation. In *Proceedings of 8th IEEE International Symposium on Intelligent Control*, 505–510. IEEE.

Grabowska, K. and Szczuko, P. (2015). Ship resistance prediction with artificial neural networks. In *2015 Signal Processing: Algorithms, Architectures, Arrangements, and Applications (SPA)*, 168–173. IEEE.

Holtrop, J. (1984). A statistical re-analysis of resistance and propulsion data. *International shipbuilding progress*, 31(363), 272–276.

IMO (2020). Fourth imo greenhouse gas study. *International Maritime Organisation (IMO)*.

Lackenby, H. (1963). The effect of shallow water on ship speed. *Shipbuilder and Marine Engine Builder*, 70(672).

Liu, X., Liu, X., Zhou, Z., and Hu, L. (2021). An efficient multi-objective optimization method based on the adaptive approximation model of the radial basis function. *Structural and Multidisciplinary Optimization*, 63(3), 1385–1403.

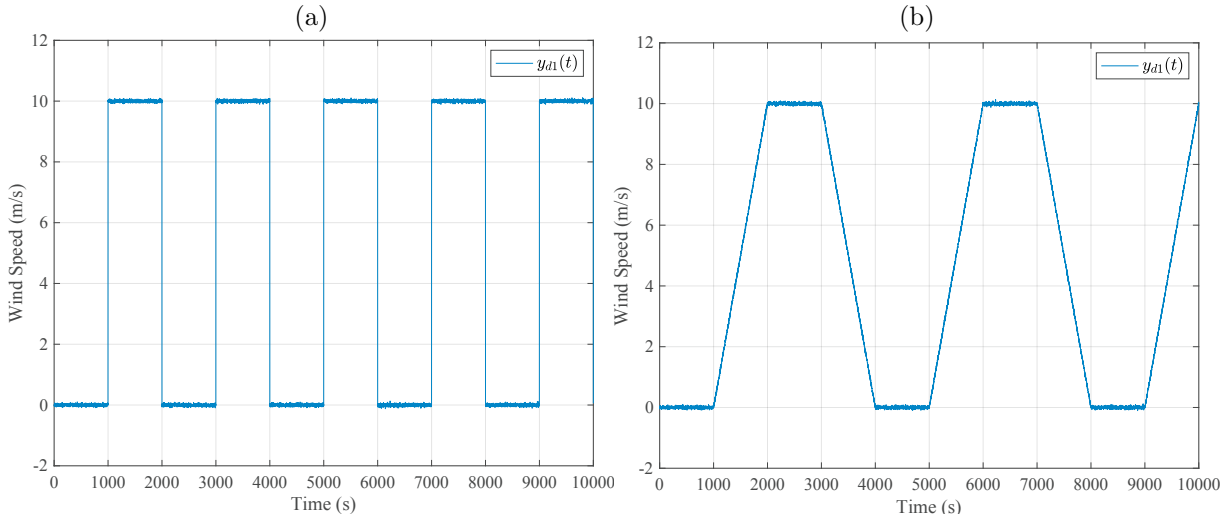

Fig. 2: Measured wind velocity $y_{d1}(t)$ input signals: (a) Pulse function, (b) Ramp function

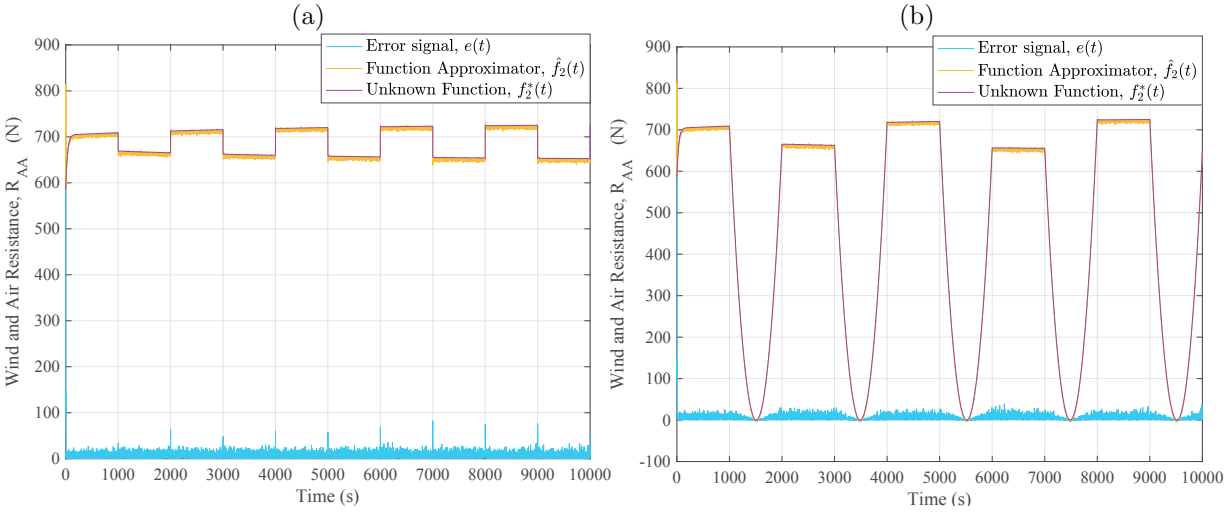

Fig. 3: Simulation results for: (a) Pulse $y_{d1}(t)$ signal, (b) Ramp $y_{d1}(t)$ signal

Miller, S.L. and Childers, D. (2012). Chapter 12 - simulation techniques. In S.L. Miller and D. Childers (eds.), *Probability and Random Processes (Second Edition)*, 517–546. Academic Press, Boston, second edition edition.

Moreira, L., Vettor, R., and Guedes Soares, C. (2021). Neural network approach for predicting ship speed and fuel consumption. *Journal of Marine Science and Engineering*, 9(2), 119.

Nikolopoulos, L. and Boulougouris, E. (2019). A study on the statistical calibration of the holtrop and mennen approximate power prediction method for full hull form, low froude number vessels. *Journal of Ship Production and Design*, 35(01), 41–68.

Nuij, G.J. (2021). Introduction of pem fuel cells on inland ships.

Pedersen, B.P. and Larsen, J. (2009). Modeling of ship propulsion performance. In *World Maritime Technology Conference WMTC2009*.

Raven, H. (2016). A new correction procedure for shallow-water effects in ship speed trials. In *Proceedings of the 13th International Symposium on PRActical Design of Ships and Other Floating Structures PRADS*.

Reppa, V., Polycarpou, M.M., Panayiotou, C.G., et al. (2016). Sensor fault diagnosis. *Foundations and Trends® in Systems and Control*, 3(1-2), 1–248.

Schlichting, O. (1934). Ship resistance in water of limited depth-resistance of sea-going vessels in shallow water. *Jahrbuch der STG*, 35, 127–148.

Wu, Y., Wang, H., Zhang, B., and Du, K.L. (2012). Using radial basis function networks for function approximation and classification. *International Scholarly Research Notices*, 2012.

Yoo, B. and Kim, J. (2017). Powering performance analysis of full-scale ships under environmental disturbances. *IFAC-PapersOnLine*, 50(1), 2323–2328.

Yoo, B. and Kim, J. (2019). Probabilistic modeling of ship powering performance using full-scale operational data. *Applied Ocean Research*, 82, 1–9.

Zeng, Q. (2019). A method to improve the prediction of ship resistance in shallow water. *Delft University of Technology*.

Zhang, Q. (2016). *Multilevel Adaptive Radial Basis Function Approximation using Error Indicators*. Ph.D. thesis, University of Leicester.